Effects of gap width on vacuum-ultraviolet transmission through submicrometer-period, freestanding transmission gratings

Matthew M. Balkey, Earl E. Scime, Mark L. Schattenburg, and Joost van Beek

The effects of gap width on the transmission coefficient of vacuum-ultraviolet light through submicrometer-period, freestanding transmission gratings are reported. Results from computations and an analytical waveguide model are shown to be consistent with experimental measurements. These results show that thin gratings with narrow gaps and thick gratings with wide gaps are equally effective at eliminating 121.6-nm radiation. The thin gratings with the narrow gaps have the advantage of better attenuation of shorter-wavelength radiation than the thick gratings with the larger gaps. © 1998 Optical Society of America

OCIS codes: 350.2770, 260.7200, 230.7380.

1. Introduction

Our interest in submicrometer-period, freestanding transmission gratings arises from their potential use as vacuum-ultraviolet (VUV) light-blocking filters in neutral-atom imaging detectors.[1,2] An effective neutral-atom imager requires the ratio of transmission coefficients for particles to 121.6-nm VUV to exceed 10^5.[1–4] A grating-based imager has the advantages of having higher sensitivity, better time resolution, and less mass than other designs.[1] Previous measurements and numerical simulations for 200-nm period gratings with 70-nm gaps and 130-nm bars[5–7] suggest that thick gratings (thickness, >700 nm) should achieve the needed rejection level. However, construction of gratings is mechanically difficult for gap aspect ratios (thickness-to-gap widths) greater than 10. To predict the VUV light transmission of a grating before construction we have developed an analytical parallel-plate waveguide model and performed numerical simulations. The simulations are consistent with the predictions of the analytical model and indicate that considerably thinner gratings with narrower gaps ($\approx$40 nm) can achieve the required VUV rejection levels. As shown here, the narrower-gap gratings have the added advantage of more effectively eliminating shorter wavelengths such as the 58.4-nm helium line. Such background-light rejection is critical for neutral-atom imaging of the Earth's magnetosphere by use of existing detector designs.[1–4]

In Section 2 the basic grating configuration is reviewed and simple equations are presented for transmission of radiation through two parallel, resistive plates to illustrate the role played by the gap width in determination of the overall transmission of TE- and TM-polarized electromagnetic radiation. In Section 3 we present results of numerical simulations for the complete grating structure, and in Section 4 we detail the experimental confirmation of the numerical simulations.

2. Grating Structure and Transmission through Parallel Plates

Our gratings were constructed at the Massachusetts Institute of Technology's Space Microstructures Laboratory by techniques developed for the Advanced X-ray Astrophysics Facility satellite.[8–10] The grating pattern is established upon a photoresist surface by an interference pattern that arises from the mixing of two beams of a 351.1-nm argon-ion laser. The resultant mask is processed further, permitting the deposition of gold between the bars of the mask. The remaining photoresist is then etched away, leav-

M. M. Balkey and E. E. Scime are with the Department of Physics, West Virginia University, Morgantown, West Virginia 26506. M. L. Schattenburg and J. van Beek are with the Center for Space Research, Massachusetts Institute of Technology, Cambridge, Massachusetts 02139.

Received 17 February 1998; revised manuscript received 17 April 1998.

0003-6935/98/225087-06$15.00/0

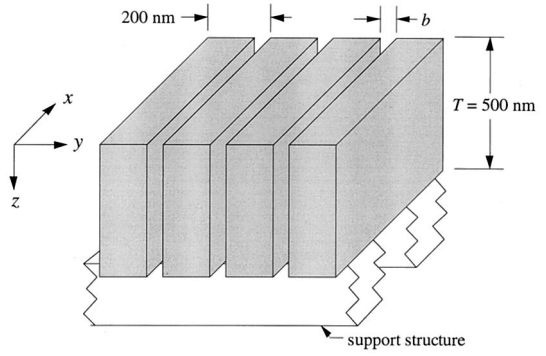

Fig. 1. Schematic of a 500-nm-thick freestanding gold grating with a 200-nm period. The shaded region is solid gold separated by vacuum. The support structure maintains the structural integrity of the grating.

ing a 200-nm period grating resting upon a layer of plating base material. Because the grating is too weak to support itself, two support gratings fabricated by ultraviolet lithography are superimposed atop the 200-nm period grating, as depicted in Fig. 1, and the plating base is etched away. The transparency of the support structure is roughly 50%, and the typical grating thickness is 500 nm.

A parallel-plate waveguide, illustrated in Fig. 2, can be used as a simple model for these gratings. Conductive boundaries are located at $y = 0$ and $y = b$, with no boundaries in the x direction. Wave propagation is along z. A semi-infinite waveguide model is physically justified because the primary wavelength of interest, 121.6 nm, is small compared with the grating thickness, measured along z, and the length, measured along x. Interference and diffractive effects, which can be significant,[11] are ignored under these assumptions.

Unpolarized light incident upon the grating can be separated into TE (electric field parallel to the conducting walls) and TM (electric field perpendicular to the conducting walls) polarizations. In the case of a perfect conductor, the TE component obeys the dispersion relation[12]

$$\left(\frac{\omega}{c}\right)^2 = k^2 + \left(\frac{n\pi}{b}\right)^2. \tag{1}$$

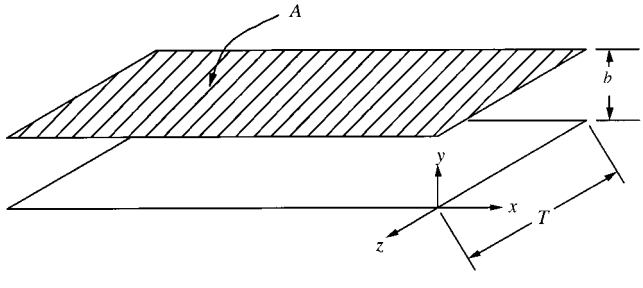

Fig. 2. Coordinate system used for the parallel-plate waveguide model. Two parallel plates are separated by gap b. A is the surface area of each of the parallel plates, T is the thickness of the waveguide, and wave propagation is in the z direction.

The integer n denotes the Fourier mode of the TE component.[12] For $\omega < \omega_c = \pi c/b$, i.e., $\lambda > \lambda_c = 2b$, $\mathbf{k}$ is purely imaginary. Below this frequency cutoff, the wavelength is too large to fit between the walls of the waveguide. Above cutoff, $\omega > \omega_c$, the wave propagates without losses through a waveguide with perfectly conducting walls. The finite conductivity of any real material causes dissipation of the wave energy owing to ohmic losses to the metal.

The power transmitted through the waveguide decays exponentially owing to resistive losses as[12]

$$P(z) = P_0 \exp(-2\beta z), \tag{2}$$

where

$$2\beta_{\mathrm{TE}} = \frac{\delta 2|n\pi|^2}{kb^3} \tag{3}$$

for the TE polarization. Here δ is the frequency-dependent skin depth. Note that the exponential dependence is proportional to $-z/b^3$. One can reduce the power transmitted through the waveguide in the TE polarization by decreasing the gap b or by increasing the thickness of the grating T. Because of the b^{-3} term, a small change in the gap width has a significantly greater effect than a comparable change in the thickness of the grating.

Below cutoff, $\omega < \omega_c$, the wave vector $\mathbf{k}$ is purely imaginary, and the fields inside the waveguide decay as $\exp(-kz)$ for perfectly conducting walls. The power transmitted through a real waveguide below cutoff decays because of the evanescent character of the wave and the resistive losses to the walls. The combination of the resistive losses to the metal walls and the evanescent character of the wave below cutoff leads to negligibly small transmitted power for radiation in the TE polarization below cutoff.

For a parallel-plate waveguide the TM polarization is the same as the free-space TEM polarization. The TEM polarization obeys the free-space dispersion relation

$$\omega/c = k, \tag{4}$$

and there are no cutoff conditions imposed by the boundaries. The only attenuation of TEM radiation is caused by resistive losses in the conductor. The transmitted power will have the same form as Eq. (2), with[12]

$$2\beta_{\mathrm{TEM}} = \delta \frac{\omega}{2cb}. \tag{5}$$

The exponential decay constant for the TEM component is proportional to $-z/b$. One can increase the resistive losses by decreasing the gap b or by increasing the thickness of the grating T. Increasing the thickness of the grating simply provides more surface area for resistive losses, but the gap effect is due to the structure of the wave fields that are responsible for the surface currents in the waveguide walls. To reduce the TEM transmission, a smaller gap is just as

effective as a thicker grating. Note that the gap effect is exponential, not the simple linear decrease in transmission that might be expected for a waveguide with a narrower opening.

Using gratings that have approximately 10% transmission for neutral atoms requires a transmission coefficient of 10^{-6} for 121.6-nm radiation for neutral-atom imaging of the Earth's magnetosphere.[1–3] A polarizer eliminates half of the incident power of unpolarized light, the TE component, by operating below cutoff. This analytical waveguide model suggests that to achieve a VUV transmission coefficient of 10^{-6} one can increase the resistive dissipation of the TEM component by using gratings with narrower gaps or by making the gratings thicker.

The background radiation reflected from the Earth's geocorona includes wavelengths shorter than 121.6-nm. The intensity at these shorter wavelengths is less than the intensity of the 121.6-nm light[13] but can generate substantial background during measurements of neutral atoms. Although the TE components at these wavelengths, such as the 58.4-nm helium line, are above cutoff for a grating with a 60-nm gap, the resistive effects of the gold grating attenuate the transmitted intensity as $\exp[-2\delta(n\pi)^2 z/kb^3]$. Previous calculations showed that, above cutoff, the transmitted power is dominated by the TE component.[5] Therefore this simple waveguide model also suggests that gratings with a smaller gap will be more effective at reducing the transmitted intensity of shorter wavelengths than thicker gratings.

3. Numerical Simulation of Grating Performance

Numerical simulations of grating transmission were performed with the three-dimensional, full-wave vector code Gsolver.[14] With this code it is possible to model a grating that has a periodicity in the y direction, is infinite in the x direction, and has a finite thickness along z. The boundary conditions at all the surfaces, the finite conductivity of gold, and reflections off the front surface of the grating are included in the computational results. Adjustable parameters include the period, the thickness of the grating, the gap between the gold bars as a function of z, the angle of polarization of the incident radiation, and the wavelength of the incident radiation. The measured index of refraction of gold as a function of wavelength was used in the calculations.[15] For neutral-atom imaging of the Earth's magnetosphere the experimental configuration of interest is unpolarized 121.6-nm light incident upon a gold grating with a period of 200 nm.[1] Transmission coefficients predicted by the waveguide model and numerical simulations are compared for various values of gap and thickness of the grating. Transmission at shorter wavelengths, primarily 58.4-nm, is also investigated.

Figure 3(a) shows the results of simulations above cutoff for 121.6-nm light incident upon a gold grating with a 200-nm period. The simulated transmission coefficient of the TE component exhibits similiar dependence on b, as predicted by the analytical model, and the TE mode dominates the overall transmission through the grating above cutoff. The waveguide model predicts a TE transmission coefficient of $5.97 \times 10^6\ b\ \exp(-3.82 \times 10^6\ \mathrm{nm}^3/b^3)$ and a TEM transmission coefficient of $5.97 \times 10^6 b\ \exp(-516\ \mathrm{nm}/b)$ above cutoff. Assuming that equal amplitudes of TE and TEM radiation enter the grating, the waveguide model predicts that the TEM mode will dominate the overall transmission for gaps less than 86 nm. For gap widths larger than 86 nm the TE component should dominate the transmission. The discrepancy between the waveguide model and the numerical simulations occurs because gold is a poor conductor at the frequency of interest, which results in a reduction of the TEM transmission. Simulations performed with indices of refraction for a good conductor yielded results for the TE and TEM components that agree with the waveguide model.

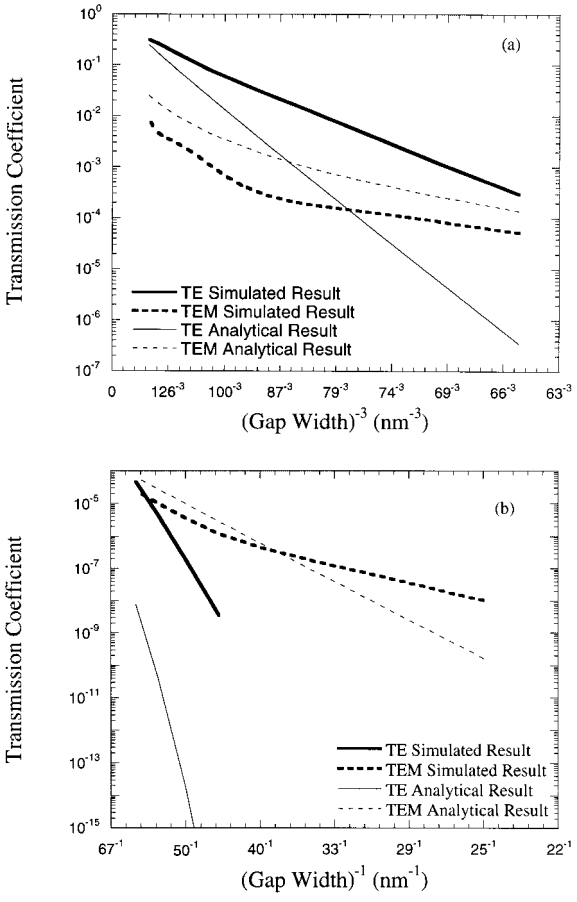

Fig. 3. Transmission coefficient as a function of gap width for 121.6-nm VUV radiation incident upon a 200-nm-period, 500-nm-thick grating, obtained through numerical simulation and analytical waveguide model calculations. (a) Above cutoff, $b > 60.8$ nm, the numerical simulation results suggest that the TE component dominates the overall transmission, whereas the analytical waveguide model suggests that the TEM component should dominate for gaps smaller than 86 nm. (b) Below cutoff, $b < 60.8$ nm, the TE component is effectively eliminated, and the TEM component falls off exponentially.

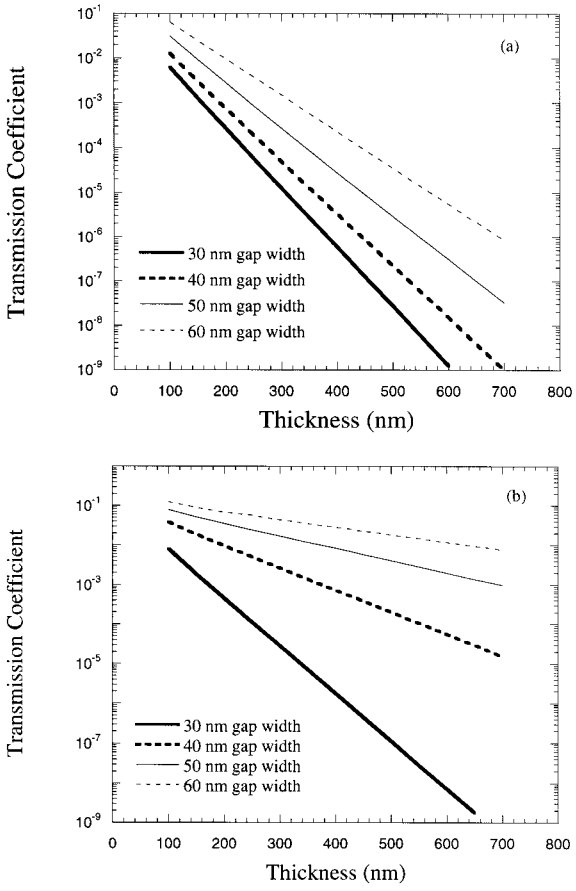

Fig. 4. Results of numerical simulations for total transmission through a 200-nm-period grating as a function of grating thickness for different gap widths. Predicted transmission coefficients for (a) 121.6-nm VUV, (b) 58.4-nm VUV.

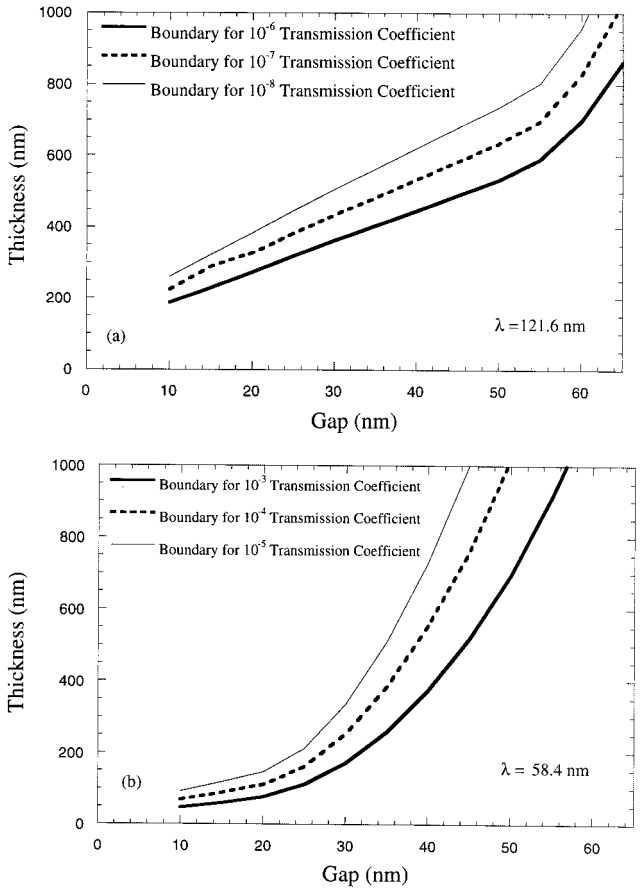

Fig. 5. Results of numerical simulations for VUV radiation incident upon a 200-nm-period grating, showing thickness-versus-gap-width curves needed for a given transmission coefficient. (a) Boundaries for 10^{-6}, 10^{-7}, and 10^{-8} transmission coefficients for 121.6-nm VUV. (b) Boundaries for 10^{-3}, 10^{-4}, and 10^{-5} coefficients for 58.4-nm VUV. Values for thickness and gap width that fall above the curves yield a transmission coefficient of less than the magnitude indicated by the curve.

Figure 3(b) shows the effects of gap width on transmission below the TE cutoff. In agreement with the waveguide model, the numerically simulated TEM component dominates the overall transmission below cutoff. However, it is not well fitted with a single $\exp(-z/b)$ type of relationship. The simulations suggest that the physics of TEM transmission below cutoff is more complicated than the physics of the simple waveguide model. However, the TEM transmission does decay exponentially as a function of $1/b$, consistent with the predictions of the waveguide model below cutoff.

To obtain the required rejection level for 121.6-nm radiation, one can use thick gratings or gratings with small gap widths. Because of limitations in the fabrication process, it is difficult to produce gratings that both are thick and have narrow gaps. Figure 4(a) shows the total transmission coefficient versus thickness for several gaps and a 200-nm period. For gratings with gaps less than $\lambda/2$ (below the cutoff for TE waves) the transmission coefficient is dominated by the TEM component, as shown in Fig. 3(b). According to Fig. 4(a), a grating with a 40-nm gap width must be 450-nm thick to achieve a 10^{-6} transmission coefficient for 121.6-nm VUV. For the same transmission coefficient of 121.6-nm VUV, a grating with a 60-nm gap must be 700-nm thick. The ratio of thickness to gap width is 11.3 for the 450-nm-thick grating and 11.6 for the 700-nm-thick grating. Therefore these two gratings are equally difficult to make and would give the same transmission of 121.6-nm VUV. As shown in Fig. 4(b), the thinner grating with the narrower gap has the advantage of better attenuation of shorter-wavelength radiation, e.g., the 58.4-nm line of helium. The numerically simulated transmission coefficients for 58.4-nm VUV are 2.6×10^{-3} for a 450-nm-thick grating with a 40-nm gap and 5.1×10^{-2} for a 700-nm-thick grating with a 60-nm gap: a result of the $1/b^3$ dependence in the exponent in Eq. (3). For construction purposes, the gap widths and thicknesses required for transmission coefficient of 10^{-6} for 121.6-nm VUV and a transmission coefficient of 10^{-3} for 58.4-nm VUV are shown in Fig. 5.

4. Experimental Transmission Measurements

A set of gratings received from The Massachusetts Institute of Technology was tested in a monochro-

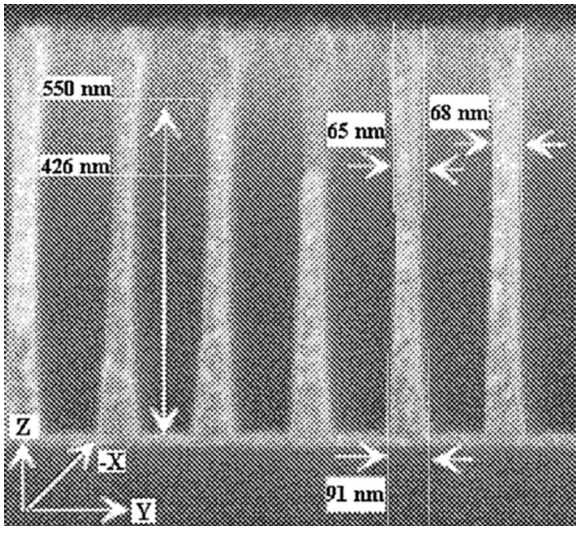

Fig. 6. SEM image of the etched channel in the photoresist material before it is filled with gold. The thickness of the grating is approximately 550 nm. Note that the gap width ranges from 91 nm at the top and the bottom to approximately 55 nm in the center.

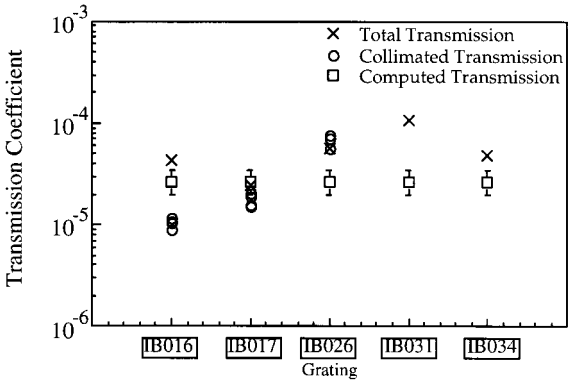

Fig. 7. Experimental measurements of 121.6-nm VUV transmission through five gold gratings. ×, transmission coefficient when the entire grating surface is illuminated. ○, transmission coefficient for a small region (approximately 2 mm in diameter) of the grating. □, numerical predictions for a typical grating based on the measurements of the gap structure in the photoresist. The numerical simulated transmission coefficients for the grating are identical because they came from the same manufacturing lot. Variations in the lot yield different measured transmission coefficients for the gratings.

matic VUV test facility built at West Virginia University.[16] The essential components of the light source are a 30-W Hamamatsu deuterium lamp with primary emission in the range 120–200 nm, two 10-nm FWHM bandpass filters with a central wavelength of 121.6 nm, an ultraviolet-to-visible conversion phosphor, and a high-sensitivity photomultiplier tube detector.

Before the etched lines in the photoresist material are filled with gold, samples are cleaved and examined with scanning-electron microscopy (SEM). A SEM image of a sample photoresist structure is shown in Fig. 6 and demonstrates the nonparallel edges of the gaps. The gap profile shown in Fig. 6 is representative of the entire set of gratings, but there are variances across each individual grating and between different gratings. On average, the set of gratings has a minimum gap of 40 nm at the midplane that widens to 70 nm at the top and the bottom. After the photoresist is filled with gold the photoresist is etched away, leaving gratings that are approximately 550 nm thick.

VUV transmission measurements of five gratings range from 9.1×10^{-6} to 1.1×10^{-4}, as shown in Fig. 7. We measured multiple values of the transmission coefficient for a given grating, using the collimator to sample small portions of the grating rather than the entire incident area (1.70 cm × 1.03 cm). The variances in the collimated results are caused by small differences in the gap across the grating surface, pinholes that arise from contamination during processing of the grating, and strain around the edge of the grating created by the gluing of the grating to a frame. The statistical error associated with each point, caused by background light, is smaller than the data point.

The agreement between the measurements and the computational results improves when the curvature of the gap is taken into account, which we accomplished by using a tiered grating model with different gap widths at different heights, as depicted in Fig. 8. The SEM image in Fig. 6 was used as a template for the model. We estimated the error bars on the computational result by using the entire range of values for the index of refraction of gold at 121.6 nm available in the published literature.[15,17,18] The average computational results are within a factor of 3 of the experimental values for gratings IB016, IB017, and IB034. The two gratings with significantly larger transmission coefficients than predicted, gratings IB026 and IB031, had clear structural problems. Grating IB026 was damaged during processing, resulting in a large hole and other light leaks. SEM images of IB031 show clumping of the gold bars. In some regions the bars are stuck together, resulting in double-wide bars and double-wide slot gaps. Ac-

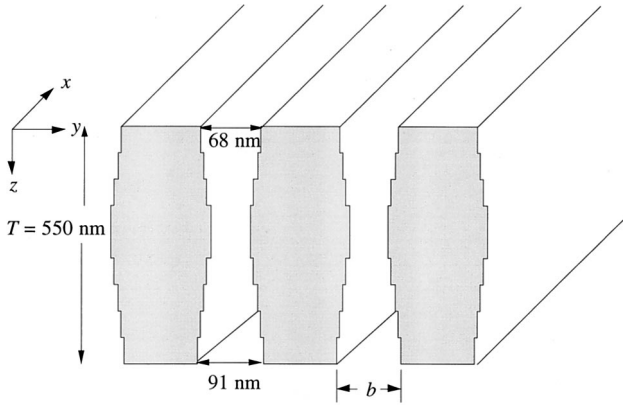

Fig. 8. Tiered model of gap in the gold grating used in computational model. The gap between the bars narrows in the middle of the grating (the reverse of the photoresist image in Fig. 6).

cording to the waveguide model, 121.6-nm VUV is above the TE cutoff for a double-wide gap. Thus the model is qualitatively consistent with the experimentally measured transmission coefficient for grating IB031.

5. Summary

The simulation of the grating performance with the Gsolver software confirmed that, below cutoff, the TEM component dominates the transmission and generally obeys an $\exp(-\delta\omega z/2cb)$ type of dependence on slot gap. Above cutoff, the simulations indicate that the TE component dominates the transmission and scales as $\exp[-2\delta(n\pi)^2 z/kb^3]$. These results are similar in character to those predicted by the analytical waveguide model, but the magnitudes of the predicted transmission coefficients in the numerical and the analytical models differ. The discrepancy is due to the fact that the waveguide model assumes that gold is a good conductor and does not account for the coupling of the incident radiation into the grating. The numerical simulations satisfy the boundary conditions at all the grating surfaces and therefore yield a quantitative prediction of the transmission coefficient. Experimental measurements of the transmission of 121.6-nm radiation through five 200-nm-period gratings are in good agreement with numerical predictions that include the detailed geometry of the gap structure. The typical VUV transmission coefficient of the gratings was 2×10^{-5}.

Based on the predictions of the waveguide model and the numerical results, the MIT group has focused its efforts on developing 500-nm-thick gratings with narrower gaps for neutral-atom imaging. The gratings with narrower gaps have less open area, so they reduce the neutral-particle transmission as well as the VUV transmission. However, the particle transmission decreases linearly with the gap width, whereas the VUV transmission falls off exponentially. In addition, the narrower slot gaps provide better rejection of shorter-wavelength radiation above cutoff because of the $1/b^3$ effect in the exponential resistive loss term of Eq. (3). Computations for gratings currently under construction predict a VUV transmission coefficient at 121.6 nm of 2×10^{-6}, an order of magnitude better than the results reported here.

This study was supported by NASA through the development of the Medium Energy Neutral Atom instrument, which will fly on the Imager for Magnetopause to Aurora Global Exploration spacecraft. We thank H. Arthur Weldon for his help in developing and in our understanding of the waveguide model; Doug Mathees, Tom Milam, and Carl Weber for their expertise in the building of the measurement apparatus; and the NIS-1 group of the Los Alamos National Laboratory for the use of its facilities for grating testing.

References and Notes

1. E. E. Scime, H. O. Funsten, M. A. Gruntman, and D. J. McComas, "Novel low-energy neutral atom imaging technique," Opt. Eng. **33,** 357–361 (1994).
2. M. A. Gruntman, "Submicron structures: promising filters in VUV—a review" in *VUV, X-Ray, and Gamma-Ray Instrumentation for Astronomy*, O. H. Siegmund and R. E. Rothschild, eds., Proc. SPIE **1549,** 385–394 (1991).
3. M. A. Gruntman, "Energetic neutral atom imaging of space plasmas," Rev. Sci. Instrum. **68,** 3617–3656 (1997).
4. D. J. McComas, H. O. Funsten, J. T. Gosling, K. R. Moore, E. E. Scime, and M. F. Thomsen, "Fundamentals of low-energy neutral atom imaging," Opt. Eng. **33,** 335–341 (1994).
5. E. E. Scime, E. H. Anderson, D. J. McComas, and M. L. Schattenburg, "Extreme-ultraviolet polarization and filtering with gold transmission gratings," Appl. Opt. **34,** 648–654 (1995).
6. M. A. Gruntman, "Extreme-ultraviolet radiation filtering by freestanding transmission gratings," Appl. Opt. **34,** 5732–5737 (1995).
7. M. A. Gruntman, "Transmission grating filtering of 52–140-nm radiation," Appl. Opt. **36,** 2203–2205 (1997).
8. M. L. Schattenburg, E. H. Anderson, and H. I. Smith, "X-ray/VUV transmission gratings for astrophysical and laboratory applications," Phys. Scr. **41,** 13–20 (1990).
9. M. L. Schattenburg, C. R. Canizares, D. Dewey, K. A. Flanagan, M. Hamnett, A. M. Levine, K. S. K. Lum, R. Manikkalingam, T. H. Markert, and H. I. Smith, "Transmission grating spectroscopy and the Advanced X-ray Astrophysics Facility (AXAF)," Opt. Eng. **30,** 1590–1600 (1991).
10. J. M. Carter, D. B. Olster, M. L. Schattenburg, A. Yen, and H. I. Smith, "Large-area, freestanding gratings for atom interferometry produced using holographic lithography," J. Vac. Sci. Technol. B **10,** 2909–2911 (1992).
11. H. Lochbihler and P. Predehl, "Characterization of x-ray transmission gratings," Appl. Opt. **31,** 964–971 (1992).
12. J. D. Jackson, *Classical Electrodynamics* (Wiley, New York, 1975), pp. 334–384.
13. R. R. Meier, "Ultraviolet spectroscopy and remote sensing of the upper atmosphere," Space Sci. Rev. **58,** 1–185 (1991).
14. Available from the Grating Solver Development Company, Allen, Tex. 75013.
15. D. E. Gray, ed., *American Institute of Physics Handbook* (McGraw-Hill, New York, 1972), pp. 6–118.
16. E. E. Scime and M. M. Balkey, "A compact, intense, monchromatic, atmospheric pressure, extreme ultraviolet light source," submitted to Rev. Sci. Instrum.
17. E. D. Palik, ed., *Handbook of Optical Constants of Solids* (Academic, New York, 1985), pp. 286–295.
18. J. H. Weaver, C. Krafka, D. W. Lynch, and E. E. Koch, "Optical properties of metals. I. The transition metals," Phys. Dat. **18,** 59–64 (1981).